Journal of Alloys and Compounds 495 (2010) 76–81

Contents lists available at ScienceDirect

Journal of Alloys and Compounds

journal homepage: www.elsevier.com/locate/jallcom

Nanocrystalline zinc oxide thin films by novel double pulse single step electrodeposition

A.I. Inamdar[a,b], A.C. Sonavane[a], S.K. Sharma[c], Hyunsik Im[b], P.S. Patil[a,*]

[a] Thin Film Materials Laboratory, Department of Physics, Shivaji University, Vidhyanagar, Kolhapur 416004, Maharashtra, India
[b] Department of Semiconductor Science, Dongguk University, Seoul 100-715, Republic of Korea
[c] Millimeter-wave Innovation Technology Research Center, Department of Electronics Engineering, Dongguk University, Seoul 100-715, Republic of Korea

ARTICLE INFO

Article history:
Received 7 November 2009
Received in revised form 15 January 2010
Accepted 19 January 2010
Available online 28 January 2010

Keywords:
Zinc oxide thin films
Electrodeposition
X-ray diffractometer
Quartz crystal microbalance (EQCM)
Transmittance electron microscopy (TEM)

ABSTRACT

An attempt has been made to fabricate nanocrystalline zinc oxide thin films by using double pulse potentiostatic electrodeposition in oxygen saturated zinc acetate bath onto FTO coated conducting glass substrates. Zinc oxide formation mechanism has been studied by using linear sweep voltammetry (LSV) and electrochemical quartz crystal microbalance (EQCM) in presence of oxygen. The influence of pulse parameters like nucleation pulse potential (E_1) and growth pulse potential (E_2) of a potentiostatic double pulse on the size distribution of zinc oxide thin films is investigated. The structural, morphological and optical properties of zinc oxide nanocrystalline thin films were studied. The results reveal how to tailor nanoparticles with respect to size, monodispersity and density of the deposit. Zinc oxide nanoparticles have been synthesized by optimizing pulse parameters of double pulse technique in oxygen saturated zinc acetate bath. The quantum size effect on optical band gap energies has been studied for the ZnO nanocrystalline thin films.

1. Introduction

Nowdays nanocrystalline zinc oxide has received considerable attention as a cost effective alternative to conventional photoelectrochemical solar cells. The synthesis of ZnO nanostructures such as nanowires, nanorods, nanosheets, nanobelts and nanotubes is of particular interest because of their high porosity and large surface area, which are essential for optimized performance of dye sensitized solar cells, sensors and hydrogen devices [1–6]. Titania (TiO_2) is typically used as the photoanode material in DSSCs [7–9]. Gratzel's group successfully developed a DSSC with a high power conversion efficiency of about 10.4% using thick spin-coated nanoporous-TiO_2 films as photoelectrode [10]. Besides TiO_2, ZnO is one of the most promising semiconductor materials in DSSCs, due to its stability against photocorrosion and similar photochemical properties to those of TiO_2 [11–16]. However, the energy conversion efficiencies of ZnO film-based DSSCs are relatively low. The reason for low efficiency is that ZnO has inherent defects that cause a decrease in the efficient effective surface area. It is well known that controlling the size of zinc oxide nanostructures, it can greatly influence the performance of the final functional devices. Therefore, the preparation of nanocrystalline zinc oxide thin films with less or no defects is a key to improve the performance of ZnO-based solar cells. ZnO nanostructure possess novel electronic and optical properties with applications such as room-temperature ultraviolet (UV) lasers, field-effect transistors, photodetectors, gas sensors, and dye sensitized solar cells [17,18]. It is reported that the chemical routes are easy and convenient for the synthesis of ZnO nanostructures [1,19–21]. Electrochemical deposition technique is convenient and fast method to deposit metals on large scale onto the conducting substrates. Here for the production of nanocrystalline ZnO thin films the double pulse electrodeposition method has been adopted. Double pulse electrodeposition method has following features: (i) production of nanocrystalline thin films without use of templates (template free), additives, capping agents and surfactants, (ii) it is fast and simple to produce nanocrystalline thin films on time scale of minute in single step as compared to conventional electrodeposition technique, (iii) uniform distribution of nuclei generated during the nucleation pulse, (iv) the seeds are generated during nucleation pulse at higher potential and growth takes place at the lower polarization and (v) the magnitude and time period of nucleating pulse facilitates control over density and size of seeds, contrast to the conventional electrodeposition process, where-in, the process is relatively straight forward and the growth parameters can only be changed by varying ex situ parameters like solution concentration, pH, etc.

This method invented by Scheludko and Todorova [22] is based on extremely short nucleation pulse of high cathodic potential followed by a much longer growth pulse at low cathodic overvoltage [23]. In this technique nucleation occurs within the first pulse and

* Corresponding author. Tel.: +91 231 2609230; fax: +91 231 2691533.
E-mail address: patilps_2000@yahoo.com (P.S. Patil).

0925-8388/$ – see front matter © 2010 Elsevier B.V. All rights reserved.
doi:10.1016/j.jallcom.2010.01.090

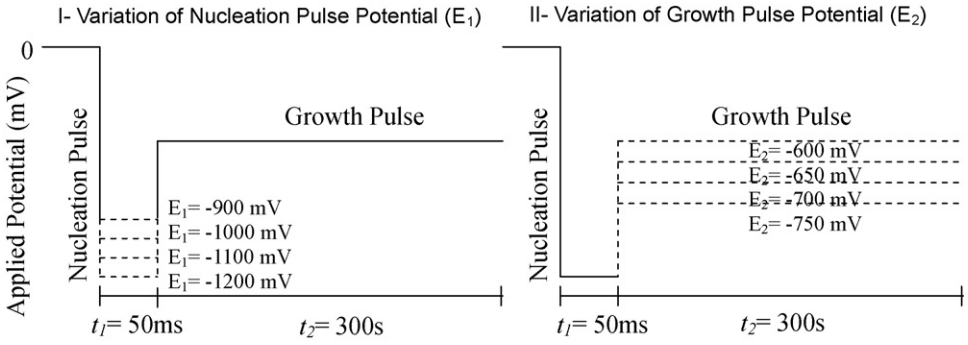

Fig. 1. Schematic for the double pulse electrodeposition by varying nucleation pulse (−900 mV to −1200 mV) and growth pulse (−600 mV to −750 mV).

exclusive particle growth in the second pulse. The high cathodic potential of the first pulse is necessary in order to initiate nucleation. For the production of metallic nanoparticles such as gold, platinum, cobalt and silver this method has been extensively used by Penner et al. [24–27]. To decrease dispersion in particle size during electrocrystallization, two important principles should be taken into account [28]. Firstly, the crystal seed formation has to occur spontaneously, thus preventing progressive nucleation. Secondly, the crystal growth has to be conducted at a slow rate, i.e. at low overvoltage.

Previously we have successfully deposited zinc oxide thin films by using conventional electrodeposition technique [18,29–31]. In the present work we have applied our previous experience and the attempt has been made to deposit zinc oxide nanocrystalline thin films by using double pulse technique. It is observed that use of electrochemical double pulse method is a convenient, fast and easy way to produce nanocrystalline zinc oxide thin films in single step. This work is focused on the development of non-template, electrochemical routes to dimensionally uniform zinc oxide nanostructures by using double pulse electrodeposition.

2. Experimental

A three-electrode electrochemical cell was used for electrochemical deposition of nanocrystalline ZnO thin films. The FTO coated conducting glass substrates (10–15 Ω/□) with an area of 3 cm^2 were used as the working electrodes, a graphite plate as a counter electrode and saturated calomel electrode (SCE) as a reference electrode (SCE E_0 = 0.244 V vs SHE, the saturated hydrogen electrode). The electrodes were placed parallel to each other separated by a distance of 2 cm. An aqueous solution of 50 mM zinc acetate (Thomas Baker, 99.5%) was used. 0.1 M KCl (potassium chloride) solution was added to it as a supporting electrolyte. During the electrodeposition oxygen gas was bubbled through the bath. Prior to the film deposition, the substrates were cleaned with soap solution in distilled water and under ultrasonic cleaner, with acetone, alcohol and finally with distilled water. EG & G versastat-II model PAR-362 was used for the deposition of nanocrystalline zinc oxide thin films in potentiostatic mode.

The schematic for the double pulse deposition is shown in Fig. 1. The pulse parameters were chosen as follows:

Nucleation pulse : $E_{1\,max} = -1200\,mV,\ E_{1\,min} = -900\,mV,\ t_1 = 50\,ms,\ t_2 = 360\,s.$

Growth pulse : $E_{2\,max} = -750\,mV,\ E_{2\,min} = -600\,mV,\ t_1 = 50\,ms,\ t_2 = 360\,s.$

In this study the nucleation pulse was varied by keeping potential of growth pulse (−650 mV vs SCE) constant for above-mentioned duration. In the second part the potential of growth pulse was varied by keeping constant potential (−1000 mV vs SCE) of nucleation pulse for the same duration. The electrochemical quartz crystal (EQCM) measurements were taken using electrochemical analyzer (Model-CHI-400A) made by CH Instrument, USA. EQCM measurements were performed onto platinum electrode of 1 cm^2 area in a specially designed electrochemical cell. A sharp step was created onto the sample and their thicknesses were measured using Ambios surface profiler (XP-1). The surface morphology of samples was observed using the JEOL-JSM 6360 scanning electron microscope (SEM). X-ray diffraction (XRD) spectra of the films were recorded by using X-ray diffractometer (Philips PW-3710) with Cu-Kα radiation of 1.5418 Å wavelength. The optical transmittance and absorption were measured by using Schimatzu make UV-VIS 3600 spectrophotometer. The films deposited by keeping growth pulse potential constant at E_2 = −650 mV and varying the deposition potential from −900 mV to −1200 mV were denoted by A1–A4, respectively whereas the films deposited with varying growth pulse from −600 mV to −750 mV were denoted by B1–B4.

3. Results and discussion

The linear sweep voltammogram was recorded in the potential range +0.2 V to −1.2 V (vs SCE) in 50 mM zinc acetate solution at 10 mV/s. Fig. 2a and b is associated with the reduction behavior of zinc species on Pt electrode (area 1 cm^2) accompanied by a concurrent shift in the frequency of the quartz crystal electrode with applied voltage.

During the cathodic scan a peak observed at −0.2 V (vs SCE) is due to oxygen reduction [18,32] and the onset of Zn^{2+} reduction is observed at −0.7 V (vs SCE), which can be seen in Fig. 1a as rise in current density and in Fig. 1b as increase in mass deposited onto the Pt electrode. The scan was terminated at −1.2 V (vs SCE). Beyond −1.2 V (vs SCE) hydrogen evolution takes place into the aqueous zinc acetate bath. According to double pulse theory the potential range E_1 and E_2 are defined as nucleation pulse potential and growth pulse potential, respectively. The shift in frequency of the quartz electrode is proportional to an increase of mass on the electrode surface [33,34]. The increase in mass leads to a decrease in frequency, and that the magnitude of the change in frequency is directly proportional to the mass change. ZnO growth takes place via intermediate steps of hydroxide formation in presence of oxygen molecules into the electrochemical bath according to the following reactions.

The formation mechanism can be summarized through following steps:

(I) Formation of OH^- ions from dissolved oxygen

$$H_2O + \frac{1}{2}O_2 + 2e^- \rightarrow 2OH^- \quad (1)$$

(II) In presence of zinc acetate following reaction takes place

$$Zn(CH_3COO)_2 2H_2O + H_2O \rightarrow Zn^{2+} + 2CH_3COOH + 2OH^- \quad (2)$$

(III) Formation of zinc hydroxide

$$Zn^{2+}O + 2OH^- \rightarrow Zn(OH)_2 \quad (3)$$

(IV) Conversion of zinc hydroxide into zinc oxide

$$Zn(OH)_2 \rightarrow ZnO + H_2O \quad (4)$$

(V) The overall reaction in presence oxygen is

$$Zn^{2+} + \frac{1}{2}O_2 + 2e^- \rightarrow ZnO \quad (5)$$

As a result of reaction (5), ZnO seeds are formed onto the substrate under the influence of nucleating pulse. The growth takes place during the second pulse. The double pulse deposited zinc

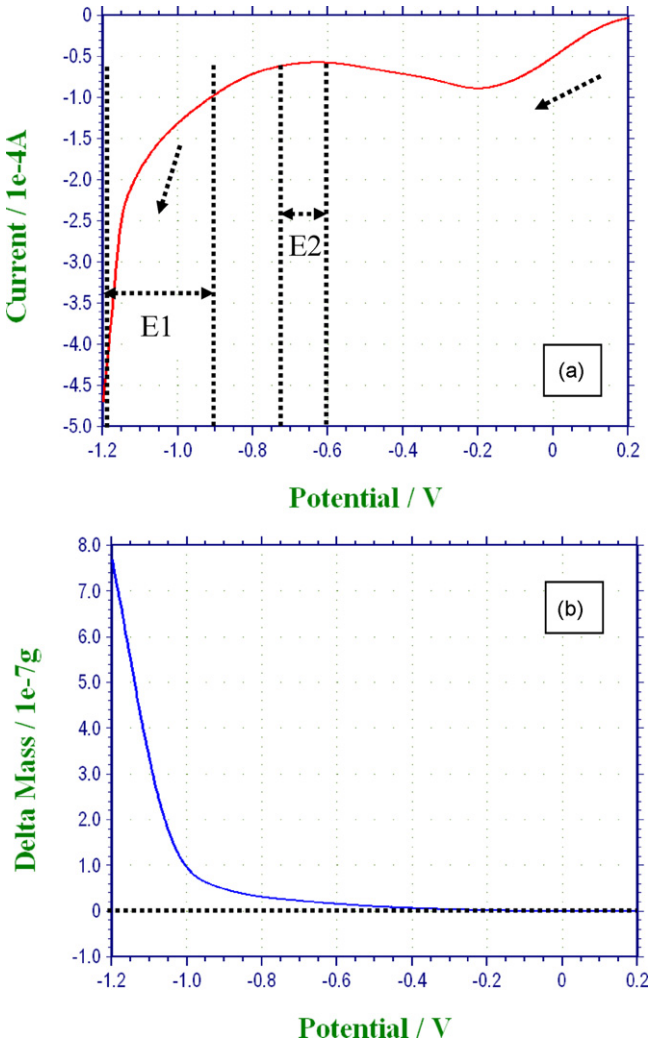

Fig. 2. Figure is associated with the reduction–oxidation behavior of the electrolyte on Pt electrode (area 1 cm^2) accompanied by a concurrent shift in the delta mass of the quartz crystal electrode with applied voltage.

oxide films are optically transparent and very thin. In order to increase the thickness of the films we have repeated nucleation and growth pulses. The thickness of all the films was optimized to be 450 nm (10 nucleation and growth pulses).

Fig. 3 shows the X-ray diffraction patterns of the films deposited at $E_1 = -1200$ (nucleation pulse potential) and $E_2 = -650$ mV (growth pulse potential) vs SCE from the precursor solution for the fixed time interval. The samples exhibit pure ZnO phase with hexagonal wurtzite structure (JCPDS Card No. 36-1533) having preferred orientation along (1 0 0). The substrate peaks are indicated by star. In addition to this one minor peak of (1 0 2) orientation at $2\theta = 47^\circ$ is observed. XRD analysis corroborates that pure and orientated zinc oxide thin films can be deposited using novel double pulse technique.

Transmittance electron microscopy (TEM) was used to reveal the grain size of zinc oxide nanostructures. TEM images of the zinc oxide thin films deposited at various nucleation pulse potential ranging from $E_{1max} = -1200$ mV to $E_{1min} = -900$ mV and $E_2 = -650$ mV for the fixed time of $t_1 = 50$ ms, $t_2 = 360$ s are shown in Fig. 4. TEM observations show the presence of nanoparticles. Fig. 4 shows the homogeneous distribution of ZnO monodispersed nanoparticles. Inset SEM images depict uniform distribution of ZnO nanoparticles onto large substrate surface. The particle size decreases slightly with increase in nucleation pulse potential (E_1)

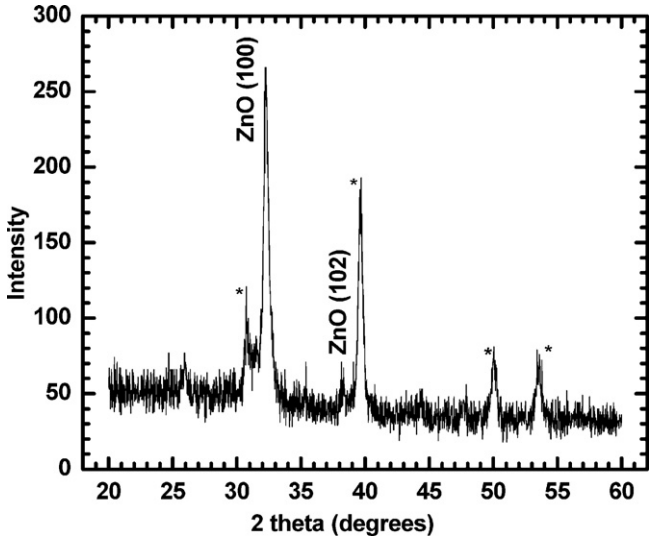

Fig. 3. XRD pattern for the film deposited by using double pulse method.

from average value 50 nm for A1 to an average of 60 nm for A4 sample.

The $E_{1min} = -900$ mV (vs SCE) is referred as critical potential (E_{CRIT}) for nanostructured nuclei formation. Below this critical potential there is no successful deposition. Similarly Ueda et al. [28] stated that on increasing the nucleation pulse potential, nucleation becomes more spontaneous and the interdependent particle growth, due to increment into the overlapping of diffusion zones. As a result, polydispersity should increase slightly but the exponential increase in particle number restricts the growth of an individual particle, i.e. the mean particle size decreases from samples A4 to A1 (Fig. 4). In the second part growth pulse potential was varied from $E_{2max} = -750$ mV to $E_{2min} = -600$ mV with fixed time of $t_1 = 50$ ms, $t_2 = 360$ s. We have kept time period constant for easy comparison. Therefore, the observed change in the particle size depends on the nature of the seed-layer formed in situ during nucleation pulse. Fig. 5 shows TEM images of the films deposited at various growth pulse potentials. Inset SEM images depict uniform distribution of ZnO nanoparticles onto large substrate surface.

TEM images represent that increase in particle size leads to increment in growth pulse potential. The average particle size varied from 50 nm for B4 to an average of 90 nm for B1 sample. It is concluded that the nanocrystalline zinc oxide thin films can be deposited by varying nucleation pulse potential (E_1) and growth pulse potential (E_2) by double pulse deposition technique.

Fig. 6 shows the variation of particle size (nm) with nucleation and growth pulse potentials which determines that as nucleation pulse potential increases above the critical potential, the particle radius decreases. The more negative the nucleation pulse potential, the narrower the particle distribution observed due to diffusion coupling of particles [28]. Also we have studied the effect of growth pulse potential on particle size of zinc oxide thin films in the range −600 mV to −750 mV. As the growth pulse potential decreases, radius of the particle decreases.

The optical properties of thin films are strongly related to their morphologies. The optical absorption and transmittance spectra of ZnO thin films were recorded in the wavelength range 300–800 nm. Fig. 7 shows the absorbance of the films deposited at various nucleation pulse potentials as −1200 mV, −1100 mV, −1000 mV and −900 mV. From the figure the sharp absorbance edge is observed in 330–370 nm range. The analysis of the edge can be performed by plotting $(\alpha h\upsilon)^2$ vs $h\upsilon$, with $h\upsilon$ being the energy of the incident light. Inset of Fig. 7 displays the band gap energy determination at zero

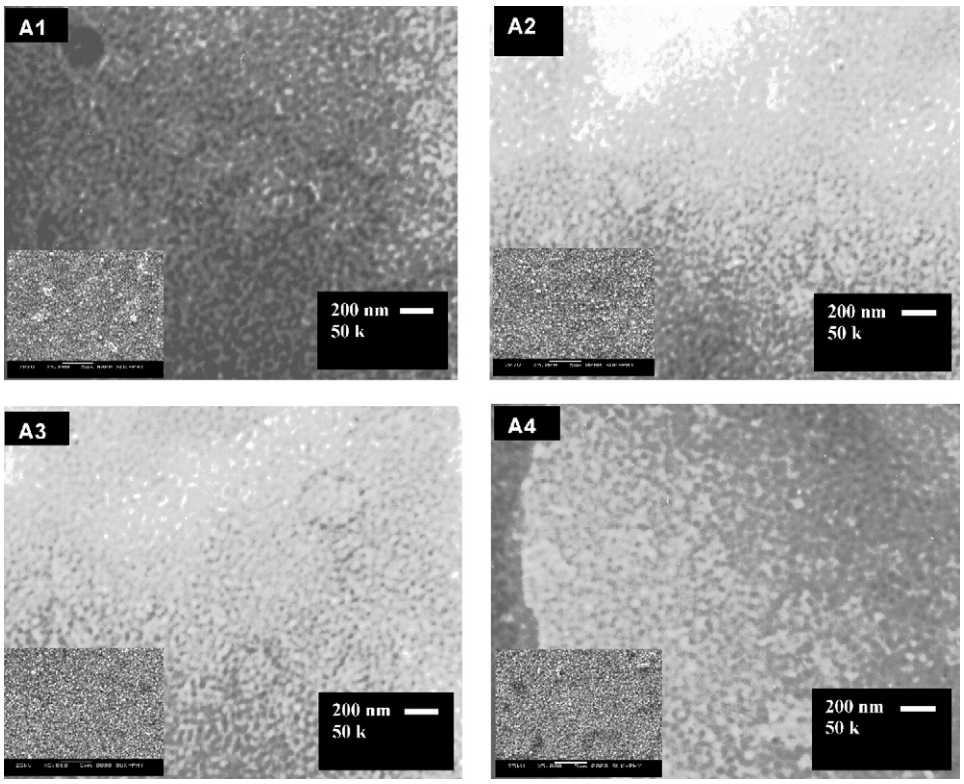

Fig. 4. TEM images for the films deposited at (A1) $E_1 = -1200$ mV, (A2) $E_1 = -1100$ mV, (A3) $E_1 = -1000$ mV and (A4) $E_1 = -900$ mV nucleation pulse potential.

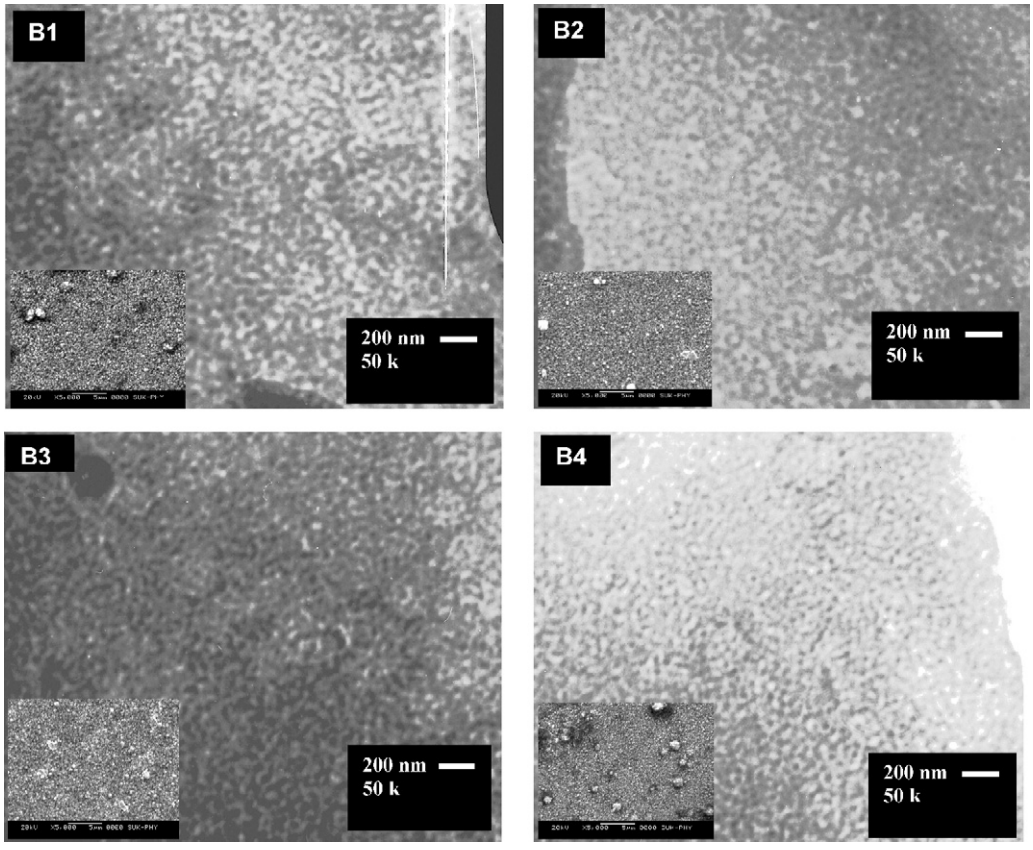

Fig. 5. TEM images for the films deposited at (B1) $E_2 = -750$ mV, (B2) $E_2 = -700$ mV, (B3) $E_2 = -650$ mV and (B4) $E_2 = -600$ mV growth pulse potential.

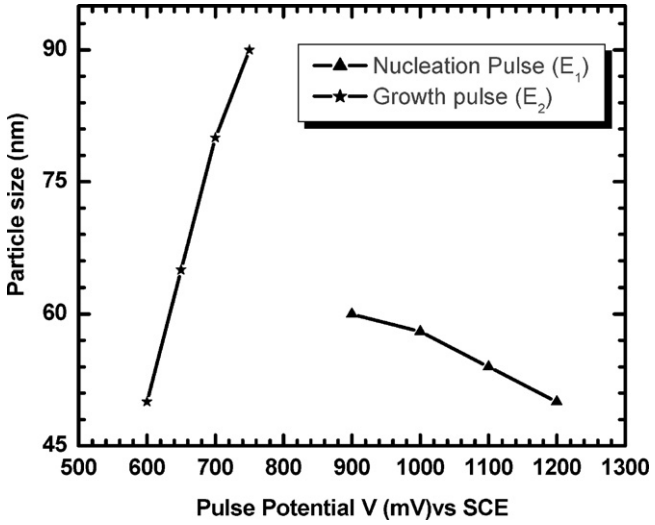

Fig. 6. The variation of particle size (nm) with nucleation and growth pulse potentials.

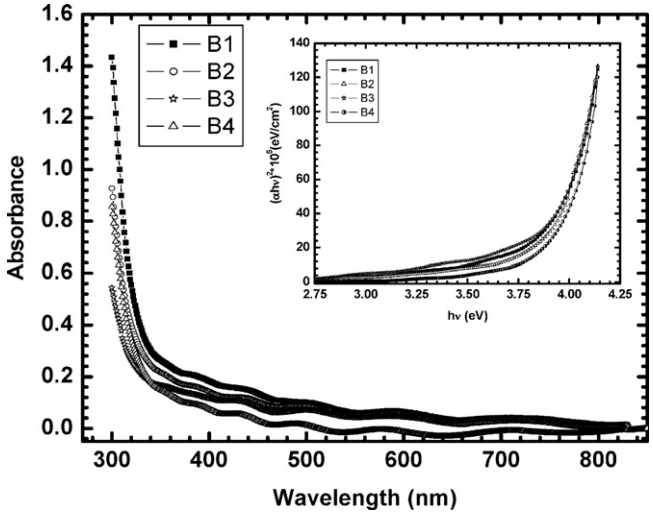

Fig. 8. Optical absorption spectra for the films deposited at (B1) $E_2 = -750$ mV, (B2) $E_2 = -700$ mV, (B3) $E_2 = -650$ mV and (B4) $E_2 = -600$ mV growth pulse.

absorption coefficients. The band gap energy for the films A1–A4 were found in the range 3.8–3.85 eV with increase in nucleation pulse potential from −900 mV to −1200 mV (vs SCE), respectively.

Similarly the absorbance for the films deposited at various growth pulse potentials are shown in Fig. 8 (B1–B4). The inset of Fig. 8 represents the band gap energy for the films deposited at various growth pulse potentials. The band gap energy is found in the range of 3.8–3.9 eV. The films deposited by double pulse technique are optically transparent. Band gap energy in the range 3.3–3.57 eV for ZnO thin films have been reported elsewhere by conventional electrodeposition technique [35].

The blueshift in the band gap energy is observed for the double pulse deposited ZnO nanocrystalline thin films. Structural changes are the responsible factor for band gap widening. Quantum confinement in semiconductor clusters offers an alternative and more fundamental explanation for the band gap widening. Possible reason for the band widening is the decrement in particle size with change in nucleation and growth pulse potentials. The widening in band gap energy as much as 1 eV is reported when going from the bulk to approximately 3 nm particle size [36,37]. Green and Hussain et al. reported that the quantum confinement contributes to the widening of band gap at small grain size [38]. The relationship between the band gap energy and the radius (R) of the particle is given as follows [39], a decrease in R results in the blueshift of band gap (E^*):

$$E* = E_g + \frac{\hbar^2 \Pi^2}{2R^2}\frac{1}{\mu'} - \frac{1.8e^2}{\varepsilon' R} \quad (6)$$

where e is the charge on electron, E_g is the band gap in the bulk, $\hbar$ is the reduced planks constant, $\hat{\varepsilon}$ is the dielectric constant of the semiconductor, $\mu'$is the reduced mass of the electron and hole.

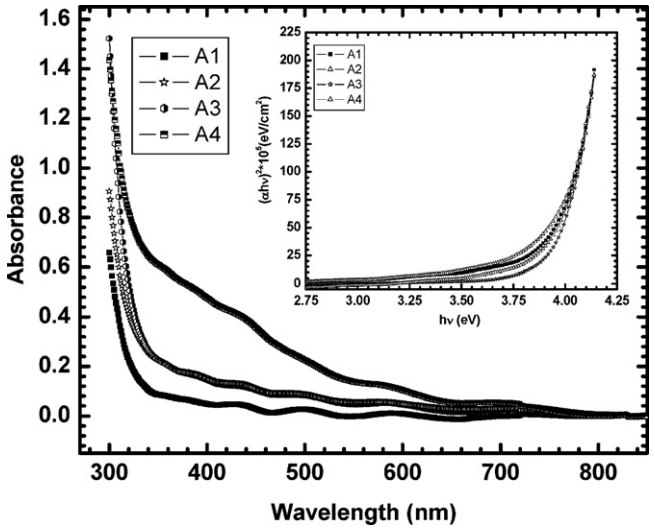

Fig. 7. Optical absorption spectra for the films deposited at (A1) $E_1 = -1200$ mV, (A2) $E_1 = -1100$ mV, (A3) $E_1 = -1000$ mV and (A4) $E_1 = -900$ mV nucleation pulse.

4. Conclusions

Nanocrystalline zinc oxide thin films has been successfully deposited by using double pulse method in oxygen saturated zinc acetate bath onto FTO coated conducting glass substrates. The ZnO thin films deposited by this technique are optically transparent, adherent and smooth. Cluster density as well as mean particle size of the deposit can be controlled by controlling the pulse parameters. With this technique, nanocrystalline zinc oxide thin films preparation is possible on a time scale of minutes. The ZnO particles with size 50–60 nm has been fabricated by varying nucleation pulse potential and the particle with size 50–90 nm has been obtained by varying growth pulse potential. One can generalize this technique to fabricate nanocrystalline oxide thin films. The effect of size on widening in the band gap energy is observed for all the films.

Acknowledgements

The authors wish to acknowledge the U.G.C., New Delhi for the financial support through the UGC-DRS IInd phase programme (2004–2009), DST through FIST programme and UGC-ASIST (COSIST) programme (2004–2010).

References

[1] X. Gana, X. Li, X. Gao, W. Yu, J. Alloys Compd. 481 (2009) 397–401.
[2] L. Feng, A. Liu, M. Liu, Y. Ma, J. Wei, B. Man, J. Alloys Compd. (2009), doi:10.1016/j.jallcom.2009.11.129.
[3] M. Willander, L.L. Yang, A. Wadeasa, S.U. Ali, M.H. Asif, Q.X. Zhao, O. Nur, J. Mater. Chem. 19 (2009) 1006–1018.
[4] K. Biswas, B. Das, C.N. Rao, J. Phys. Chem. C 112 (2008) 2404–2411.
[5] Q. Xiao, S.P. Huang, J. Zhang, C. Xiao, X.K. Tan, J. Alloys Compd. 459 (2008) L18–L22.
[6] C.F. Lin, H. Lin, J.B. Li, X. Li, J. Alloys Compd. 462 (2008) 175–180.

[7] X. Fan, Z. Chu, F. Wang, C. Zhang, L. Chen, Y. Tang, D. Zou, Adv. Mater. 20 (2008) 592–595.
[8] Y. Alivov, Z.Y. Fan, Appl. Phys. Lett. 95 (2009) 063504-1–063504-3.
[9] M. Gratzel, J. Photochem. Photobiol. C: Photochem. Rev. 4 (2003) 145–153.
[10] B. O'Regan, M. Gratzel, Nature 353 (1991) 737–740.
[11] K. Yuan, X. Yin, J. Li, J. Wu, Y. Wang, F. Huang, J. Alloys Compd. 489 (2010) 694–699.
[12] E. Guillen, C.F. Lorenzo, R. Alcantara, J.M. Calleja, J.A. Anta, Sol. Energy Mater. Sol. Cells 93 (2009) 1846–1852.
[13] X. Sheng, Y. Zhao, J. Zhai, L. Jiang, D. Zhu, Appl. Phys. A: Mater. Sci. Process. 87 (2007) 715–719.
[14] S. Rani, P. Suri, P.K. Shishodia, R.M. Mehra, Sol. Energy Mater. Sol. Cells 92 (2008) 1639–1645.
[15] D. Wei, H.E. Unalan, D. Han, Q. Zhang, L. Niu, G. Amaratunga, T. Ryhanen, Nanotechnology 19 (2008) 424006-1–424006-5.
[16] J.C. Bernede, Y. Berredjem, L. Cattin, M. Morsli, Appl. Phys. Lett. 92 (2008) 083304-1–083304-3.
[17] Z.L. Wang, Mater. Sci. Eng. R 64 (2009) 33–71.
[18] A.I. Inamdar, S.H. Mujawar, V. Ganesan, P.S. Patil, Nanotechnology 19 (2008) 325706-1–325706-7.
[19] Chenglin Yan, Dongfeng Xue, Longjiang Zou, J. Alloys Compd. 453 (2008) 87–92.
[20] Chung-Liang Cheng, Jia-Syu Lin, Yang-Fang Chen, J. Alloys Compd. 476 (2009) 903–907.
[21] J.H. Kim, E.M. Kim, D. Andeen, D. Thomson, S.P. Den Baars, F.F. Lange, Adv. Funct. Mater. 17 (2007) 463–471.
[22] A. Scheludko, M. Todorova, Bull. Acad. Bulg. Sci. Phys. 3 (1952) 61–76.
[23] G. Sandmann, H. Dietz, W. Plieth, J. Electroanal. Chem. 491 (2000) 78–79.
[24] J.V. Zoval, R.M. Stiger, P. Biernacki, R.M. Penner, J. Phys. Chem. 100 (1996) 837–844.
[25] H. Liu, R.M. Penner, J. Phys. Chem. B 104 (2000) 9131–9139.
[26] J.V. Zoval, J. Lee, S. Gorer, R.M. Penner, J. Phys. Chem. B 102 (1998) 1166–1175.
[27] M. Anderson, S. Gorer, R.M. Penner, J. Phys. Chem. B 101 (1997) 5895–5899.
[28] M. Ueda, H. Dietz, A. Anders, H. Kneppe, A. Meixner, W. Plieth, Electrochim. Acta 48 (2002) 377–386.
[29] A.I. Inamdar, S.H. Mujawar, S.B. Sadale, A.C. Sonavane, M.B. Shelar, P.S. Shinde, P.S. Patil, Sol. Energy Mater. Sol. Cells 91 (2007) 864–870.
[30] A.I. Inamdar, S.H. Mujawar, P.S. Patil, Int. J. Electrochem. Sci. 2 (2007) 797–808.
[31] A.I. Inamdar, S.H. Mujawar, S.R. Barman, P.N. Bhosale, P.S. Patil, Semicond. Sci. Technol. 23 (2008) 085013-1–085013-6.
[32] L. Vaysière, K. Keis, A. Hagfeldt, S.E. Lindquist, Chem. Mater. 13 (2001) 4395–4398.
[33] D.A. Buttry, M.D. Ward, Chem. Rev. 92 (1992) 1355–1379.
[34] G.Z. Sauerbrey, Z. Phys. 155 (1959) 206–222.
[35] S. Peulon, D. Lincot, J. Electrochem. Soc. 145 (1998) 864–874.
[36] Y. Zhang, J.K. Bailey, C.J. Brinker, N. Raman, R.M. Crooks, C.S. Ashley, Proc. Soc. Photo Opt. Instrum. Eng. 1758 (1992) 596.
[37] H. Weller, B. Bunsenges, Phys. Chem. 97 (1993) 630.
[38] M. Green, Z. Hussain, J. Appl. Phys. 69 (1991) 7788–7796.
[39] N. Satoh, T. Nakashima, K. Kamikura, K. Yamamoto, Nat. Nanotechnol. 3 (2008) 106–111.